ACS Catalysis

pubs.acs.org/acscatalysis

Research Article

The Evolution of the Acylation Mechanism in β-Lactamase and Rapid Protein Dynamics

Clara F. Frost, Dimitri Antoniou, and Steven D. Schwartz*

Cite This: ACS Catal. 2024, 14, 13640−13651

Read Online

ACCESS | Metrics & More | Article Recommendations

ABSTRACT: β-Lactamases are a class of well-studied enzymes that are known to have existed since billions of years ago, starting as a defense mechanism to stave off competitors and are now enzymes responsible for antibiotic resistance. Using ancestral sequence reconstruction, it is possible to study the crystal structure of a laboratory resurrected 2−3 billion year-old β-lactamase. Comparing the ancestral enzyme to its modern counterpart, a TEM-1 β-lactamase, the structural changes are minor, and it is probable that dynamic effects play an important role in the evolution of function. We used molecular dynamics simulations and employed transition path sampling methods to identify the presence of rate-enhancing dynamics at the femtosecond level in both systems, found that these fast motions are more efficiently coordinated in the modern enzyme, and examined how specific dynamics can pinpoint evolutionary effects that are essential for improving enzymatic catalysis.

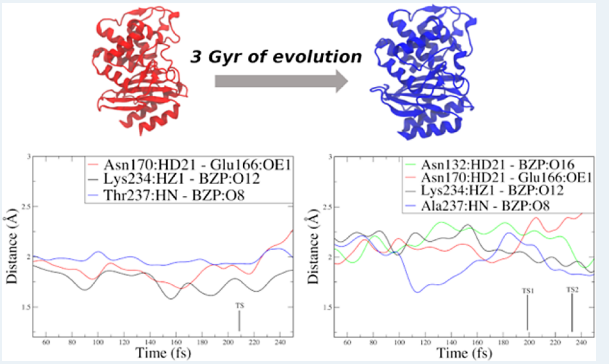

KEYWORDS: *computational chemistry, enzyme evolution, β-lactamase, transition path sampling, electric field*

INTRODUCTION

Understanding the role of protein dynamics in enzymatic catalysis continues to be a topic of contention, particularly pertaining to the role of dynamics during the chemical step.[1,2] There are two distinct types of dynamics that can affect catalysis: slow conformational motions and fast femtosecond motions that have a similar time scale to chemical barrier crossing. The outcomes of these discussions may have strong implications for protein engineering. Artificial enzyme design has continued to advance, in part due to the successful applications of directed evolution, and further identification of the atomic mechanistic details that are the outcome of evolution can be crucial. Evolutionary mutations can give insight into the role of dynamics in catalysis. In earlier work, we found that femtosecond rate promoting motions were present in the fully evolved structures of the directed evolution of artificial retro-aldolase enzymes, while absent from the less evolved structures.[3] The structures with rate promoting motions show the highest catalytic rates compared to those of the rest of these artificial enzymes. Uncovering the mutations that improve function will prove to be essential to synthesizing enzymes that can compete with the catalytic rates of natural enzymes.

To continue our previous work, we turn to the natural evolution of a reconstructed ancestral enzyme. Studying ancestral enzymes has been successful in the past and has contributed to understanding the dynamic properties that maintain their role over billions of years.[4−7] Ancestral enzymes tend to have larger active sites and slower catalytic rates and are often promiscuous, while modern enzymes are specialized.[5,8] It has been suggested that evolution of conformational motions is crucial to the development of substrate specificity.[1] In the present work, we analyze two structures of β-lactamases. It is estimated these enzymes originated more than 3 billion years ago, and they are still primarily responsible for antibiotic resistance. Several Precambrian class-A β-lactamases have been sequentially reconstructed, including one from an ancestral Gram-negative bacteria enzyme (GNCA).[9] We analyzed the effects of protein dynamics in catalysis of the ancestral GNCA and a class-A TEM-1 β-lactamase, both shown in Figure 1.

Even though there are many amino acid mutations between the ancestral GNCA and modern TEM-1 β-lactamase,[9,10] within the active site there are no significant structural changes. This enzyme pairing was chosen due to the similarities in the active sites (which makes it easier to decouple structural from dynamical effects) and their function in terms of substrate

Received: May 24, 2024
Revised: August 12, 2024
Accepted: August 20, 2024

https://doi.org/10.1021/acscatal.4c03065
ACS Catal. 2024, 14, 13640−13651

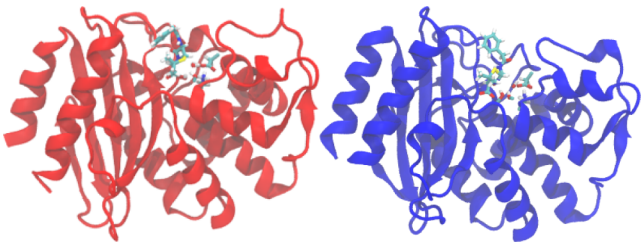

Figure 1. Nearly identical equilibrated structures of the ancestral GNCA enzyme (red) and a modern TEM-1 β-lactamase (blue) with the substrate benzylpenicillin in their respective active sites.

specificity. TEM-1 strongly prefers penicillin substrates, yet GNCA has nearly identical catalytic rates for multiple antibiotics including penicillin and CTX.[9,10] In addition, TEM-1 β-lactamase degrades penicillin at an activity 2 orders of magnitude higher than that of the ancestral GNCA.[10,11] Understanding the catalytic mechanism and rates of ancestral versus extant enzymes can provide insights that pinpoint essential and natural evolutionary changes in catalysis.

β-Lactamases break down antibiotics such as penicillin by hydrolyzing the β-lactam ring rendering the antibiotic inactive.[12] The first step in the reaction mechanism, the acylation step, is a two-step process: formation of a tetrahedral intermediate; then acylation of that intermediate.[12−14] The second step is a deacylation reaction that returns the enzyme to its initial state by hydrolyzing the acylenzyme.[15] The deacylation mechanism is well understood;[12] however, the specific mechanism to obtain the tetrahedral intermediate, the "preacylation" step, is a point of contention. Multiple pathways have been suggested due to the possibility of the catalytic base being Glu166 or Lys73. There is both experimental and computational evidence that the initial catalytic water hydrogen transfers to Glu166,[14] but other recent computational and potential energy studies suggest that the first transfer goes through Lys73.[16,17] The details of this acylation step are challenging to identify experimentally. For this study, we focus solely on the two steps that make up the acylation mechanism.

We will briefly summarize previous work on this system that identified evolutionary changes in (a) slow conformational motions and (b) electric fields in the active site.

Previous studies on reconstructed ancestral β-lactamases propose that evolutionary changes and ancestral promiscuity result from differences in conformational dynamics.[10,11] Ozkan et al. suggested that mutations that can lead to the evolution of conformational dynamics are expected to alter substrate specificity. By mutating the ancestral GNCA enzyme residues with low flexibility, they changed the previously promiscuous ancestral enzyme to a substrate-specialized enzyme.[10] One region of low flexibility that has been well studied and present throughout the evolved species is the Ω-loop, found at the opening of the active site.[18,19] This loop acts as the entrance to the active site and is responsible for the positioning of several key residues such as the catalytic base Glu166 and an active site residue Asn170.[18] This evidence of changes in conformational dynamics in the two species raises the possibility that there may be changes in rapid dynamics too.

Other work studying the evolutionary changes in β-lactamases focuses on the evolvability of electric fields. This topic continues to give insight toward understanding enzymatic catalysis, as Boxer and coworkers have shown there is a correlation between the strength of the electric field and the catalytic rate enhancement of an enzyme, and both are related to substrate configuration and rigidity.[20−22] Within β-lactamases, the active sites are highly charged, and an oxyanion hole stabilizes the anion of the tetrahedral intermediate as a result of the first part of the acylation step. As the tetrahedral intermediate is formed after the Ser70 nucleophile attacks the C7═O8 carbonyl on the β-lactam ring, the oxyanion hole stabilizes the negative charge on the O8 oxygen.[7,8] This oxyanion hole in TEM-1 β-lactamase relies on the amide hydrogens of Ala237 and Ser70. Boxer et al. studied the differences in the electric field within TEM-1 β-lactamase and an ancestral penicillin-binding protein, with penicillin-G as a substrate in the former and an inhibitor in the latter. It is suggested that proteins evolve with mutations that increase the size of the electric field in the active site to better catalytic function.

In the present work, we will examine how the evolution of this enzyme may have affected important femtosecond-level dynamics that influence the function of the ancestral and modern enzymes. Such rapid femtosecond dynamics has been found to impact the catalytic step in several systems providing evidence of a link between dynamics and catalysis.[23−26] In collaboration with experimentalists, we have shown that isotopically heavy enzymes can lower the coupling of dynamics to barrier passage and in turn lower rate.[27] In earlier work, we have seen how the presence of rate-enhancing fast dynamics in laboratory evolved enzymes plays a critical role in the function of those enzymes.[3,28,29] In more recent studies, we have shown how dynamics affects free energy barriers in engineered enzymes,[30] as well as how a coupling between conformational motions and promoting vibrations shape free energy barriers.[31] Other authors have found that the evolution of dynamic networks enhances catalysis.[32]

We employed transition path sampling (TPS)[33] and found that there are important rapid atomic motions that are present in the modern TEM-1 enzyme but missing from the reconstructed ancestral GNCA system for the formation of the tetrahedral intermediate. As we will discuss later, the key residues important for function are conserved at the active site, so the changes we observed are completely dynamic in nature. The presence of these coordinated fast atomic motions suggests further explanations for the changes in the specificity and increased catalytic rate of the extant enzyme. As mentioned above, there is evidence that the changes in function are affected by slow conformational dynamics, and this work suggests that rapid dynamics also plays a role.

RESULTS AND DISCUSSION

We generated hundreds of unbiased reactive trajectories through transition path sampling for both GNCA and TEM-1 enzymes. Transition path ensembles were generated for each enzyme to analyze both steps of the acylation process: the formation of the tetrahedral intermediate and the formation of the acylenzyme. Through a computational analysis of the generated transition path ensembles, we identified the residues that make up the reaction coordinate for both systems. The same reaction mechanism was observed in each enzyme, albeit with differences in dynamics on the femtosecond time scale. We also found differences between the electric field projected along the same dipole on the substrate benzylpenicillin's C15═O16 carbonyl, found adjacent to the β-lactam ring. Below, we detail the findings of the differences for both steps between the ancestral enzyme and its modern counterpart in

https://doi.org/10.1021/acscatal.4c03065
ACS Catal. 2024, 14, 13640−13651

terms of the atomic details of the mechanism, reaction coordinates, rapid dynamics, and electric fields.

Step 1 − Formation of the Tetrahedral Intermediate. As previously mentioned, the reaction mechanism for the formation of the tetrahedral intermediate is still debated. The results from our unbiased transition path sampling trajectories for both the ancestral and modern enzymes validate the older accepted reaction pathway with Glu166 as the initial catalytic base. Even though our results show the first step with Glu166 as the catalytic base, we should mention there is an alternative opinion, a pathway through Lys73.[16,17] The results in this work suggest the mechanism shown in Figure 2.

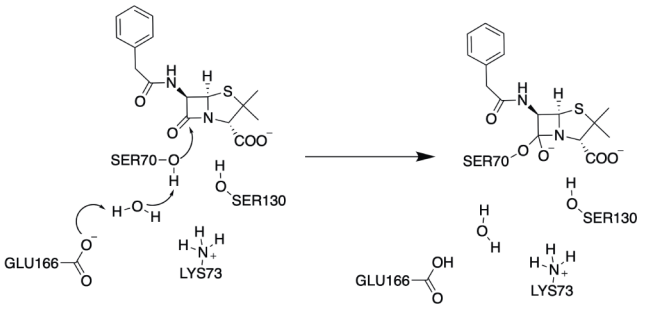

Figure 2. Mechanism of the formation of the tetrahedral intermediate. Two proton transfers through the catalytic water from Ser70 to Glu166, and a nucleophilic attack of the Ser70 oxygen at the carbonyl on the beta-lactam ring.

Our transition path sampling analysis identified the mechanism for the first step of acylation (the "preacylation step") as follows: Ser70 loses a proton to the catalytic water; Glu166 acts as the catalytic base and accepts a hydrogen from the catalytic water. This is followed by the nucleophilic attack of the deprotonated Ser70 oxygen at carbon of the benzylpenicillin carbonyl on the lactam ring.

Transition States. We identified the transition states in reactive trajectories using transition path sampling and committor analysis. The results show that the ancestral GNCA enzyme has concerted proton transfers, whereas the modern TEM-1 β-lactamase has sequential transfers. This is illustrated by the reactive trajectories for the ancestral and modern enzymes for the preacylation step shown in Figure 3:

In the ancestral enzyme, there is one primary transition state. In the modern enzyme, there are two isocommittor points: the first isocommittor point involves the two hydrogen transfers between Ser70, the catalytic water, and Glu166; the second isocommittor point isolates the nucleophilic attack of the Ser70 oxygen, which we label OGX, as it forms a bond with the benzylpenicillin carbon C7 found on the beta lactam carbonyl. This second point generally occurs around 30 fs after the first.

Reaction Coordinates. Using TPS and committor analysis,[34] we identified the reaction coordinates for both the ancestral and modern β-lactamases. For the ancestral GNCA enzyme, the set of reaction coordinate residues consist of benzylpenicillin, Ser70, Ser130, Glu166, and Lys73 (these form the QM region of our simulations) and also the residues Asn132, Pro167, Lys235, Gly236, and Thr237. The commitment probability distribution histogram is shown in Figure 4.

The modern enzyme has two isocommittor points, meaning that we need to identify reaction coordinate residues for two transition states. The first reaction coordinate contains the following residues: the QM region mentioned above, Asn132, Pro167, Lys234, Gly236, and Ala237. This is identical to the set in the ancestral enzyme except for the mutation of Ala237 from Thr237. The reaction coordinate residues for the second transfer consist only of the QM region residues. Figure 5 shows the commitment probability distributions labeled with the reaction coordinate residues for the first sequential transfer, TS1, and the second transfer TS2.

The reaction mechanism for the formation of the tetrahedral intermediate remains the same from the ancestral enzyme to extant TEM-1. The roles of the reaction coordinate residues have been well studied for the entire acylation step. All identified sets of reaction coordinate residues surround the substrate and the QM region.

Three residues that are consistently part of the reaction coordinates for both systems are Asn132, Lys234, and Thr/Ala237.

Asn132 interacts with the O16 carbonyl oxygen of the substrate and also with the QM residues Ser130, Lys73, and the catalytic water, which is crucial for substrate binding and

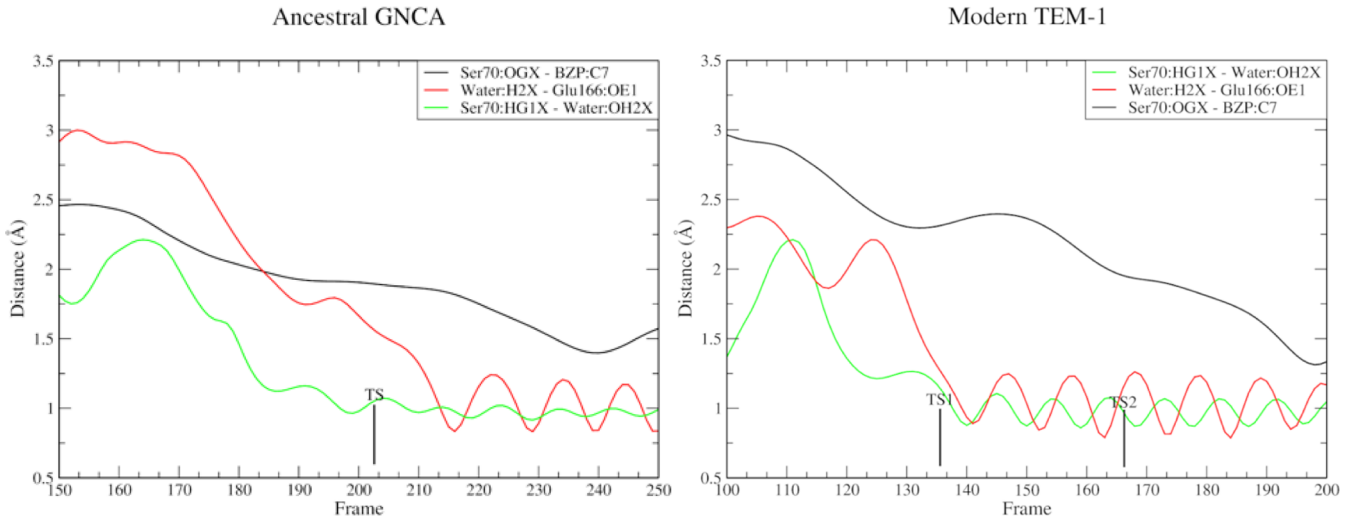

Figure 3. Reactive trajectories of the ancestral (left) and modern (right) enzymes for 100 fs. Multicolored lines indicate the distance between acceptor and donor atoms: the two proton transfers are red and green, and the Ser70 nucleophilic attack is black.

https://doi.org/10.1021/acscatal.4c03065
ACS Catal. 2024, 14, 13640−13651

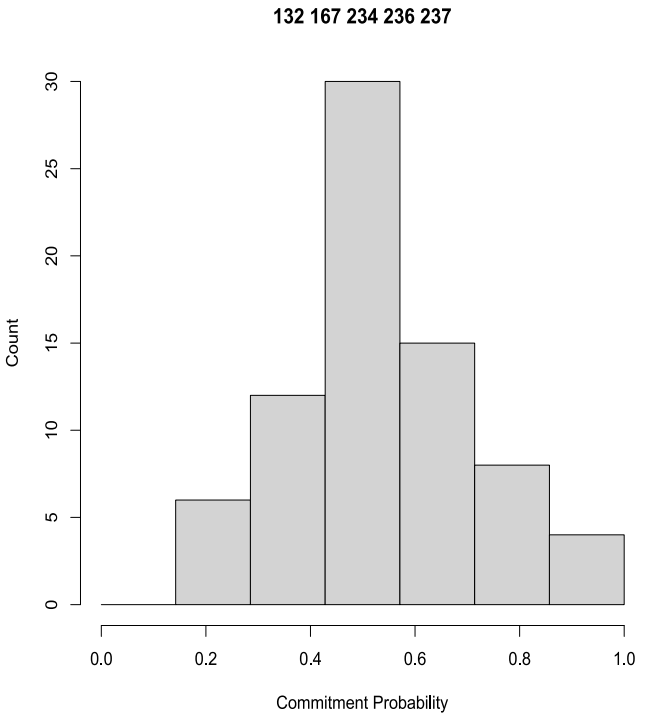

Figure 4. Committor distribution probability histogram for the ancestral GNCA enzyme. The constrained residues that make up the reaction coordinate are listed above the histogram, and the QM region listed in the text is included as well.

positioning in the active site.[12] In the ancestral GNCA enzyme, Asn132 does not interact with the same oxygen, O16, due to the difference in substrate orientations. However, it still remains a key residue as it stabilizes the active site, particularly through interactions with Lys73.

Lys234 contributes to stabilizing the tetrahedral intermediate by forming an anchor cavity for the carboxylate side chain of the substrate.[14,35]

Thr/Ala237 forms a bond with Gly236 to form the oxyanion hole. The amide backbone nitrogen is essential for acylation.[13] This is the primary mutation found in the active site, as the ancestral contains threonine, a polar hydrophilic residue, and the modern has alanine, a nonpolar hydrophobic residue. Ala237 backbone amides interact with the TEM-1 β-lactam ring bound carbonyl. This residue 237 serves as a hydrogen-bond donor in both the ancestral GNCA enzyme and the modern TEM-1 enzyme. Mutations by Boxer et al. from TEM-1 to TEM-52 show that improved alignment of the C7═O8 bond, the carbonyl on the β-lactam ring, with the backbone amides generates larger electric fields.[13] These mutations led to expansion of the active site to accommodate other β-lactam antibiotics, such as CTX, in these studies. These results heavily imply that the role of Thr237 in the ancestral enzyme contributes to its promiscuity.

The remaining residues are Gly236 and Pro167. The Gly236 residue forms a peptide bond with Ala and Thr237 as part of the oxyanion hole. The backbone amide hydrogens stabilize the carbonyl oxygen O8, and it stabilizes the transition state.[12,13] Pro167 is a part of the omega loop, which has a wide range of implications at slower time scales.[14,18,19] The Pro167 is suspected to fix Glu166, the catalytic base, at the precise moment for the chemical step. The rigidity, even at rapid time scales, is expected to be responsible for the positioning required for this reaction.[36] All of the reaction coordinate

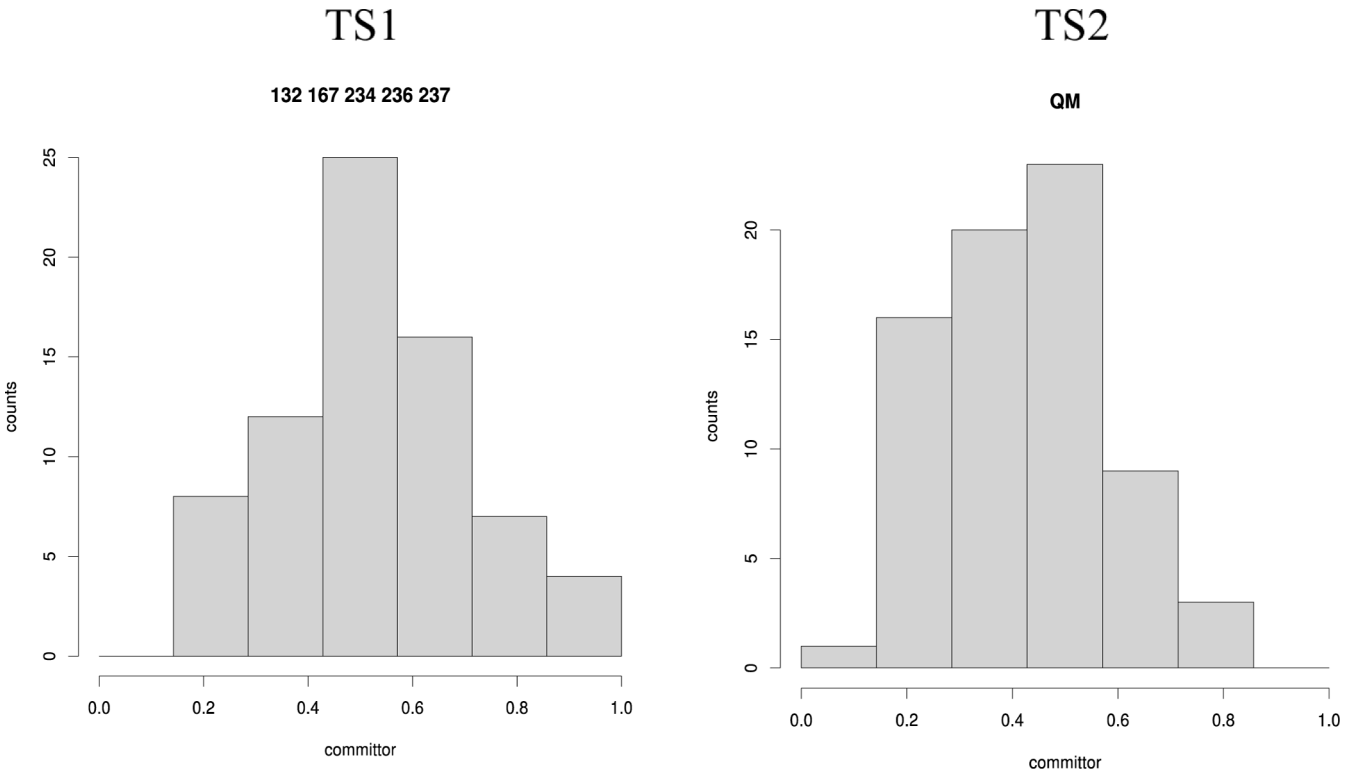

Figure 5. Committor distribution histograms for the modern TEM-1 β-lactamase. The first isocommittor point histogram is given on the left and the second on the right. The constrained residues that make up the reaction coordinate are listed above each histogram, with the QM residues included for the first isocommittor point as well.

https://doi.org/10.1021/acscatal.4c03065
ACS Catal. 2024, 14, 13640−13651

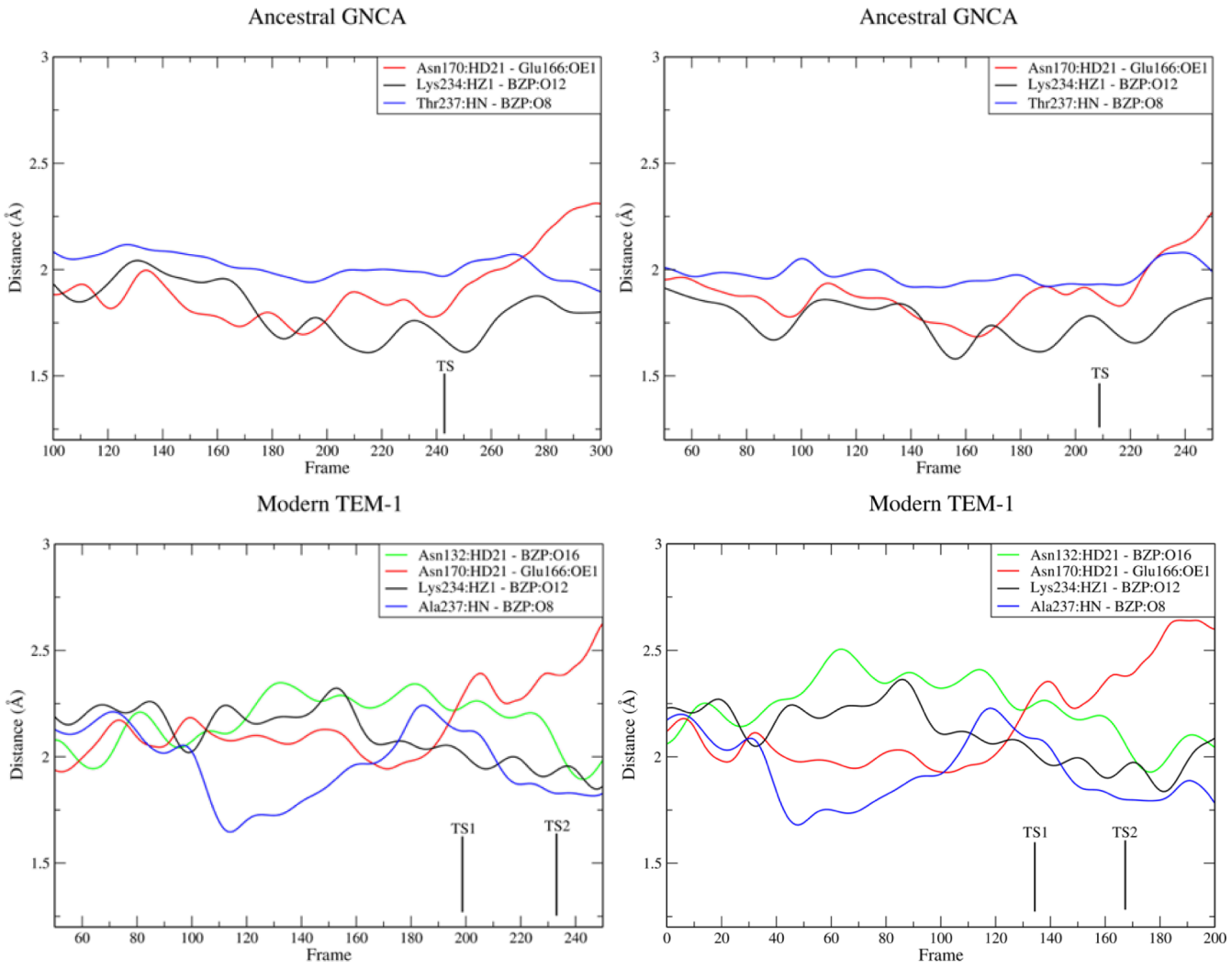

Figure 6. Distances between 4 of the identified reaction coordinate residues and their corresponding bonds to the substrate benzylpenicillin over the course of 200 fs in the ancestral enzyme (top) and modern TEM-1 (bottom). Asn132 (green) is not seen in the ancestral enzyme due to its distance to the substrate oxygen being greater than 3 Å.

residues found are essential for the reaction to occur, but they vary greatly in dynamics across the evolution of the ancestral GNCA to modern TEM-1 enzyme.

Dynamics. We analyzed the dynamical information gathered from the generated TPS trajectories and found that there are significant differences between the dynamics present in the two active sites for this preacylation step that forms the oxyanion. We show the movements between the hydrogen bonds of four reaction coordinate residues and the substrate throughout transition state formation in both the ancestral and modern enzymes.

Ancestral Enzyme. It shows low mobility, as seen in Figure 6. Lys234 has the smallest distance between the residue and the substrate in the ancestral enzyme, reaching a bond length of around 1.7 Å 30 fs before the transition state as it interacts with the benzylpenicillin oxygen O12 while forming the anchor cavity. The bond between Asn132 and the substrate oxygen O16 does not reach below 3 Å and is not seen in Figure 6 for the ancestral enzyme.

Modern Enzyme. The distances of the hydrogen bonds between the catalytic residues Asn132, Asn170, Lys234, Ala237, and benzylpenicillin oxygens for the modern TEM-1 enzyme are also shown in Figure 6. We see significant dynamics present in the modern enzyme before the transition state as Asn170 forms a hydrogen bond with Glu166, but it remains static within the ancestral enzyme's active site.

Over the course of 200 fs leading to the reaction event, the residues in the ancestral enzyme remain nearly static compared with the extant TEM-1 β-lactamase. Ala237 in particular forms a hydrogen bond with the O8 oxygen of the C7═O8 carbonyl about 100 fs before the first transition state occurs in the modern enzyme. As the bond breaks, the carbonyl becomes polarized promoting the nucleophilic attack for the second transition state. While the reaction mechanism and structure of the active site remained constant over the course of 3 billion years of evolution, clearly there was a significant increase in rapid dynamics. The presence of rapid dynamics and increased substrate specificity imply a possible connection between the presence of rate-enhancing rapid dynamics and increased substrate specificity, as well as increase the catalytic activity by 2 orders of magnitude.

Electric Fields. Lastly, for the preacylation step, we calculated the electric field along a dipole in the active site for both the modern and ancestral structures. To study the effect of the active site electric field in the ancestral and modern β-lactamases, we analyze a carbonyl found on the

https://doi.org/10.1021/acscatal.4c03065
ACS Catal. 2024, 14, 13640−13651

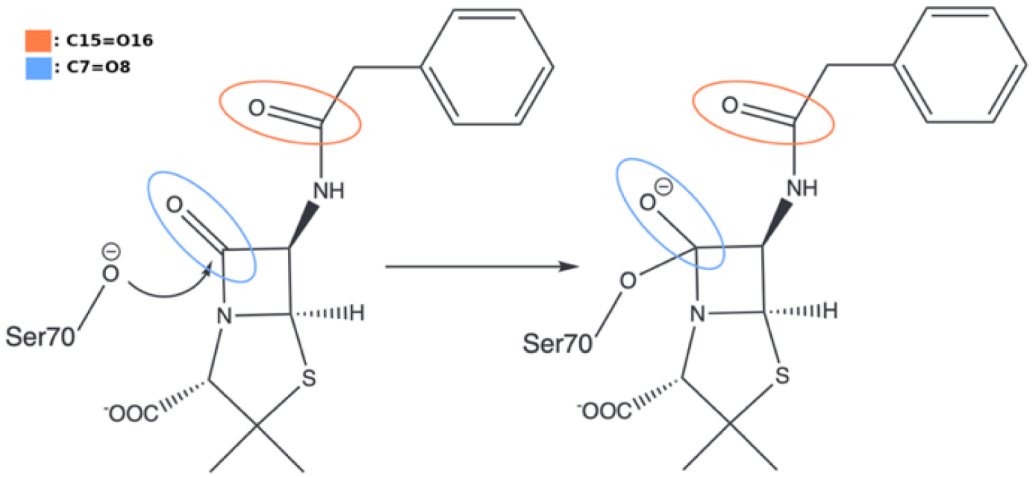

Figure 7. Reorientation of the C7═O8 carbonyl during the nucleophilic attack. C7═O8 is circled in blue, and C15═O16 is circled in orange. Electric field calculations were done on C15═O16.

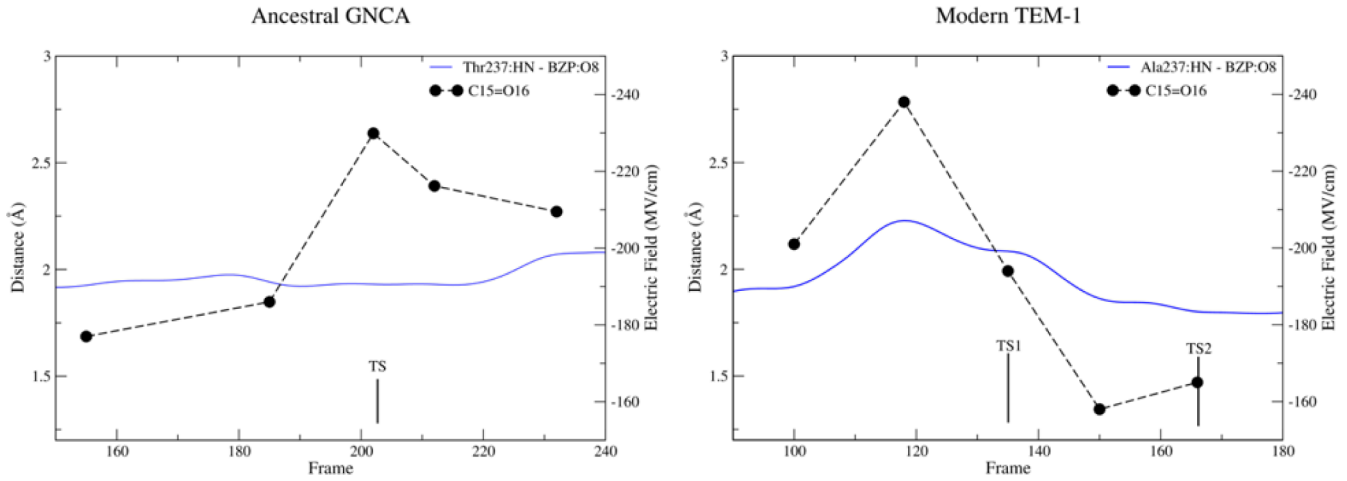

Figure 8. Electric field projected on the C15═O16 carbonyl found on the substrate benzylpenicillin for the ancestral (left) and TEM-1 (right) enzymes. The Mulliken charges were calculated and projected along the dipole at points before, during, and after the transition state(s). The electric field overlays the distance between the 237 residue and the O8 oxygen.

substrate, which we labeled C15═O16. The β-lactam ring carbonyl C7═O8 is a part of the reaction mechanism and is significantly reoriented as the tetrahedral intermediate is formed, resulting in an oxyanion. Figure 7 shows the reorientation that prevents C7═O8 from being suitable for our electric field calculation and also shows the C15═O16 carbonyl.

To get an accurate dipole approximation, we calculate the electric field on the C15═O16 carbonyl as this group remains rigid with little reorientation and is the only substrate carbonyl group suitable for this calculation.[37]

Figure 7 shows the electric field projected along the dipole throughout transition state formation. The ancestral enzyme peaks at −230 MV/cm in the transition state. In the modern enzyme, the electric field peaks at −238 MV/cm, 17 fs before the first transition state. The size of the electric fields is larger than those determined experimentally (140−175 MV/cm).[35] Our calculations are slightly limited due to both a non-polarizable force field, resulting in higher calculated values for electric fields, and the dipole approximation for the field. While there are significant advances in polarizable force fields,[38,39] this is not something we can apply using the CHARMM force field, more advanced field modeling is probably not warranted. While the peak electric field of the modern enzyme is only 8 MV/cm greater, the effect of the active site electric field is quite different. The active site residues are nearly static in the ancestral enzyme, while the motions in TEM-1 vary greatly and form hydrogen bonds with several benzylpenicillin oxygens. This provides a possible explanation for both the minor difference in magnitude and the role of the electric field itself in each case.

In the ancestral enzyme, due to the lack of dynamics, the peak in the electric field is an effect of the chemical reaction, as Ser70 attacks the β-lactam ring carbonyl. In the modern enzyme, the dynamics causes the electric field to drive the formation of the transition state. The polarization of the β-lactam carbonyl that correlates with the dynamics of Ala237 shown in Figure 8 coincides with the peak of the electric field in the modern enzyme, beginning around 12 fs before the first transition state. The stabilizing effect of the Ala237 amide hydrogen on the O8 benzylpenicillin oxygen decreases as the distance between the two becomes larger, contributing to the sudden increase of the electric field.

Additionally, the orientation of the benzylpenicillin in the active site of the ancestral enzyme and the Ser70, Thr237, and Asn132 residues contribute to the highly polarized carbonyls.

https://doi.org/10.1021/acscatal.4c03065
ACS Catal. 2024, 14, 13640−13651

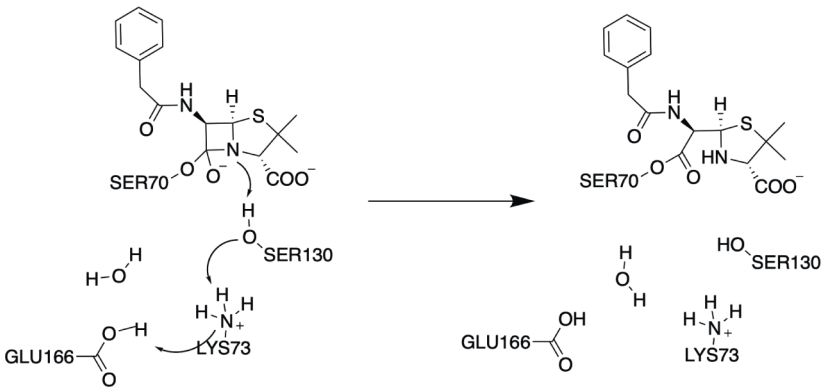

Figure 9. Mechanism of the acylation of the tetrahedral intermediate. Multiple proton transfers from Glu66 to Lys73, Lys73 to Ser130, and Ser130 to the benzylpenicillin nitrogen on the β-lactam ring.

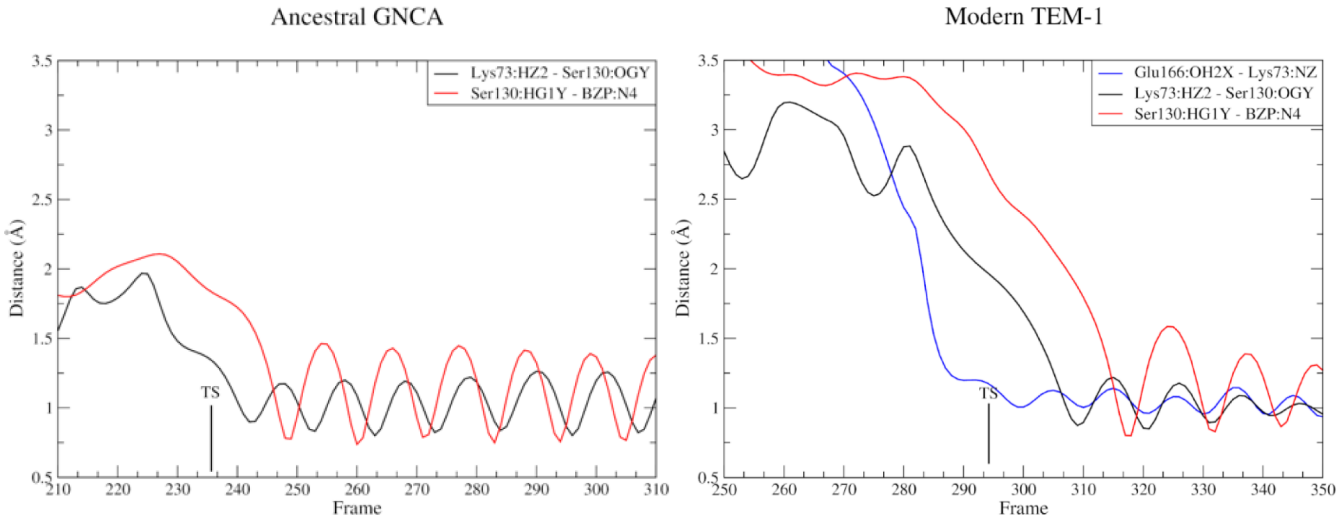

Figure 10. 100 fs showing the formation of product bonds and the transition states for the ancestral (left) and modern (right) enzymes.

The modern enzyme's residue contribution of the amide hydrogens stabilizes these charges, resulting in a similar-sized electric field. While there are correlations with a stronger electric field contributing to an enzyme's catalytic rate, in this ancestral GNCA enzyme, there are less electrostatic stabilizing bonds than in the modern TEM-1 due to the orientation of the substrate. This calculation points to the conclusion that while the size of the electric field matters, timing and orientation along a reaction coordinate are also critical.

Step 2 – Acylation of the Tetrahedral Intermediate. To complete the acylation mechanism, we took the tetrahedral intermediate formed in the first step and performed transition path sampling on the second step that results in the acylation of the tetrahedral intermediate. The second step also includes multiple proton transfers but is less debated than the first part of the oxyanion formation. The scheme showing the acylation is shown in Figure 9: Lys73 donates a proton to Ser130, and it receives a proton from Glu166, and the nitrogen we labeled "N4" takes the Ser130 proton. Once the acylenzyme is formed, the beta-lactam ring breaks between the N4 nitrogen and the C7 carbon.

Transition States. The reactive trajectories generated through transition path sampling are slightly different between the ancestral and modern enzymes. We started the sampling method with the tetrahedral intermediate as our reactant. In the ancestral, Glu166 immediately loses the H2X atom to Lys73, as Lys73 donates a proton to the other Glu166 oxygen and remains protonated. This happens before the next transfer of the Lys73 hydrogen to Ser130 as shown in Figure 10: the modern enzyme does show the initial transfer of Glu166 hydrogen to Lys73. In both cases, the proton transfers occur essentially instantaneously within 10 fs of each other.

Reaction Coordinates. The reaction coordinates calculated for this second step in the acylation mechanism were nearly identical to those for the first step. The two steps contain all of the same catalytically relevant residues, and it fits that the reaction coordinate residues are the same as well. In the ancestral, we see the same exact reaction coordinate residues as the first step: the QM region, Asn132, Pro167, Lys235, Gly236, and Thr237. For the modern enzyme, we see only one change in the reaction coordinate residues; the QM region, Asn132, Asn170, Lys235, Gly236, and Ala237. The roles of the residues from step 1 stay the same, and Asn170 is accounted for, as well.

Asn170 is directly related to the catalytic water and Glu166[14] and is not found as a reaction coordinate residue in the modern enzyme. Glu166 is the catalytic base and its catalytic role is essential for the reaction, particularly pertaining to the ester hydrolysis.[13,40] Studies show that Asn170 coordinates with Ser70, Glu166, and the catalytic water and is required for the enzyme to hydrolyze a penicillin substrate at a wild-type level catalytic rate.[41]

https://doi.org/10.1021/acscatal.4c03065
ACS Catal. 2024, 14, 13640−13651

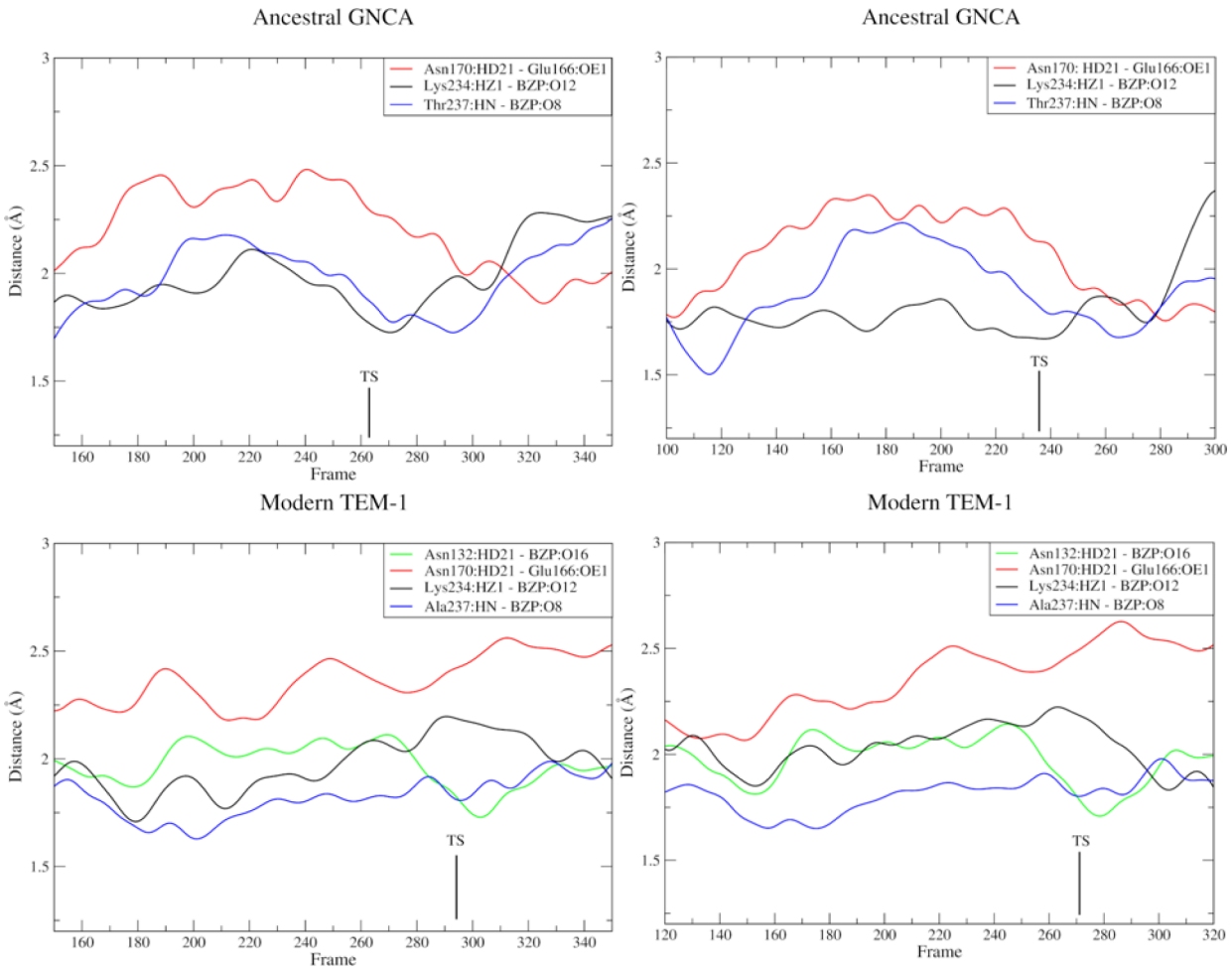

Figure 11. Distances between 4 of the identified reaction coordinate residues and their corresponding bonds to the substrate benzylpenicillin over the course of 200 fs in the ancestral enzyme (top) and modern TEM-1 (bottom) for the acylation of the tetrahedral intermediate.

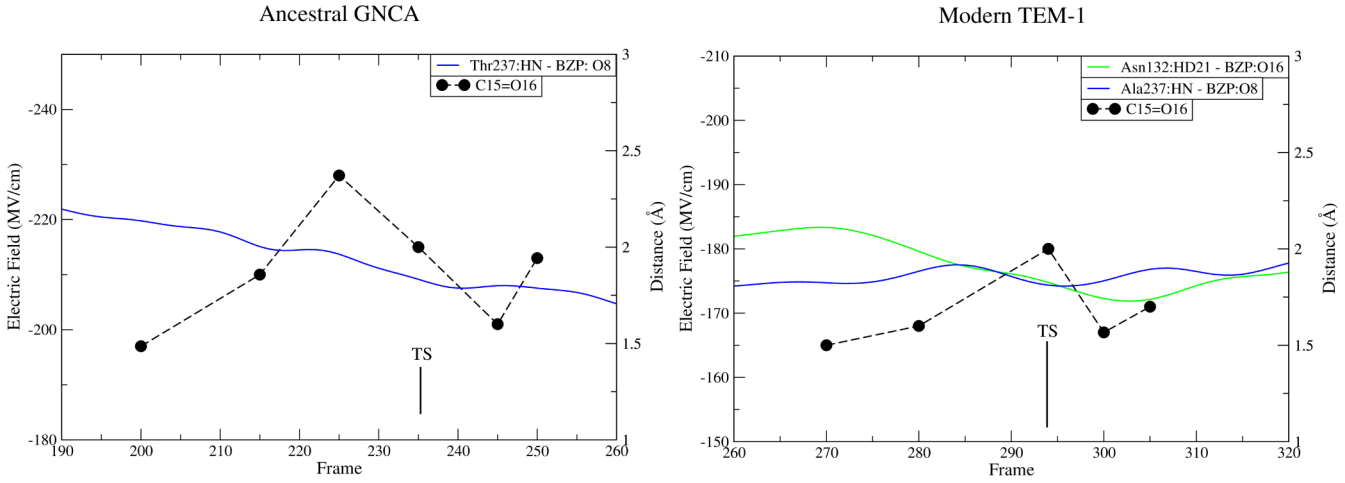

Figure 12. Electric field projected on the C15═O16 carbonyl found on the substrate benzylpenicillin for the ancestral (left) and TEM-1 (right) enzymes for the second step. The electric field overlays the distance between the 237 residue and the O8 oxygen in the ancestral, and the Asn132 residue and O16 in the modern as well.

Dynamics. As the reaction coordinates remained the same, we calculated the distances between the same atoms as in the preacylation step. The results shown in Figure 11 are dramatically different than those in the first step and between the two enzymes.

The ancestral one clearly has more dynamics in this second step than the first. Particularly, Thr237; it moves closer to the substrate 100 fs before the transition state and after the transition state. Thr237 is known to stabilize the O8 oxyanion, and the dynamics present after the transition state is when the oxyanion forms a double bond with C7 during the acylation

https://doi.org/10.1021/acscatal.4c03065
ACS Catal. 2024, 14, 13640−13651

step. Lys234 is also a part of the oxyanion hole, and we see dynamics present with that specific residue in the ancestral enzyme. We do not see this same motion from Ala237 in the modern enzyme or Lys234, although the same mechanism occurs. Ala237 is much more static in this step along with Asn170 and Lys234. The main change from step 1 is that we see Asn132 move toward the substrate right after the transition state. Once again, the distance between Asn132 and O16 is above 3 Å in the ancestral enzyme, so that is why it is not shown in Figure 11.

As the mechanism evolved over time, we see that the dynamics present are different for the ancestral and the modern enzyme. In the first step of acylation, the ancestral enzyme active site is static, and the modern involves dynamics. In the second step, it is almost reversed as the modern enzyme is nearly static except for Asn132. This potentially plays a role in the differences in specificity, as for the modern enzyme once the tetrahedral intermediate is formed the enzyme is primed for the following steps to lead to breaking the β-lactam ring. In the ancestral enzyme, however, penicillin is not the only possible antibiotic, and as the enzyme accounts for other substrates, this second step is not as readily available.

Electric Fields. Finally, we repeated the process to calculate the electric field projected along the C15═O16 dipole for the second step. There is a significant difference between the two enzymes as well as compared to the electric fields in the first step. The results are shown in Figure 12.

We see in the ancestral enzyme that for the acylation of the tetrahedral intermediate, the electric field peaks before the transition state, at −228 MV/cm. In the modern enzyme, the electric field peaks in the transition state at −180 MV/cm. In the first step, the modern enzyme peaks before the transition state as a result of the dynamics seen as residue Ala237 moves toward the benzylpenicillin O8 oxygen. In this second step, the ancestral enzyme shows an increased presence of dynamics concurring with this peak in the electric field before transition state formation. In both steps, the enzyme that has dynamics drives the electric field, while the enzyme that lacks dynamics shows that the electric field is driven by the chemical reaction itself.

The modern enzyme electric field is much lower than in step 1, and this is most likely due to the Asn132 hydrogen moving close to the O16 oxygen that we calculate the projection along. This is not seen in the first step or in the ancestral enzyme, and this stabilizing effect explains the lower electric field value.

CONCLUSION

The evolutionary path followed by β-lactamases shows how mutations both specialized and increased enzymatic efficiency. This was accomplished at least partially through the introduction of protein dynamics. The results show that modest changes in the active site structure are augmented by changes in the body of the protein, which causes the development of rapid protein motion. This in turn can mold the dynamic electrostatic environment to optimize the modern enzyme.

The evolutionary changes uncovered through this transition path sampling study showed differences among transition state formations, reaction coordinate residues, and electric fields in the ancestral GNCA enzyme and its extant TEM-1 β-lactamase for both steps in the acylation mechanism. Despite the minor structural changes, the mobility of the active site in the modern enzyme plays a significant role in the effect of the electric field. In the ancestral enzyme, the peak in the electric field corresponds to the effects of the chemical reaction for the formation of the tetrahedral intermediate. The modern enzyme, however, presents that the dynamics is responsible for the peak in the electric field as it corresponds to the polarization of the β-lactam ring carbonyl before the nucleophilic attack during the same step. The reverse is seen during the acylation of the tetrahedral intermediate, as the presence of dynamics in the ancestral GNCA during this step also shows the electric field peaking before the transition state. All of these differences have a level of correlation to the presence of rate-enhancing dynamics found in the modern enzyme and missing from the ancestral. We suggest that these results have significant implications for the field of protein engineering in terms of creating specialized enzymes and rate enhancing catalysts. Clearly, the second step of this reaction does not happen without the first. This suggests that free energy barriers associated with the first step are at least partially controlled by rapid promoting vibrations in the modern enzyme, allowing the second step to occur. The values of free energy barriers for both steps in these enzymes are unknown and are a current investigation in our group using our unbiased TPS methodology.[42]

METHODS

System Preparation. We started with the crystallized structure from the Protein Data Bank with PDB ID: 4b88 for the ancestral GNCA enzyme and PDB ID: 1fqg for the modern TEM-1 β-lactamase. The modern enzyme contained the benzylpenicillin substrate, while the ancestral GNCA was in its apo form. To add the benzylpenicillin substrate to GNCA, it was copied from the modern structure into the active site using Schrödinger Maestro.[43]

This structure is an intermediate with the nucleophilic Ser70 oxygen (OGX) and benzylpenicillin carbon (C7) bond at 1.89 Å, so we had to minimize our crystal structure to return it to a prereactant state. All methods employ the CHARMM42 program.[44,45] Structures were solvated by placing the protein with the substrate into a water sphere with the TIP3P water model.[46,47] Neutralization was accomplished by placing 9 sodium ions within the system. Minimization followed, through 50 steps of steepest descent and then 2000 steps of the adopted basis Newton−Raphson (ABNR) method. The minimized structure showed the distance between Ser70 oxygen OGX and benzylpenicillin's C7 to be 3.23 Å, which returned the initial intermediate structure to a reactant state.

We apply the QM/MM method and so partitioned the system into two regions, QM and MM. QM residues were treated with the semiempirical method AM1, which has shown successful applications in these systems.[12] The boundary atoms were treated with the general hybridized orbital (GHO) method,[48] and the QM region included 70 atoms consisting of the substrate benzylpenicillin and residues Ser70, Ser130, Glu166, and Lys73 shown in Figure 12. The boundary atoms for these 4 residues are labeled as follows: Ser70:CBX, Ser130:CBY, Glu166:CD, and Lys73:CB. The classical (MM) residues were treated with the CHARMM36 Force Field.[47] The parameters for the substrate benzylpenicillin were generated using Discovery Studio.[49]

Once the system was prepped with both QM/MM regions, it was slowly heated to 300 K, beginning with 15 ps of harmonic constraints excluding the TIP3P water molecules and hydrogen atoms, followed by 5 ps of small harmonic

https://doi.org/10.1021/acscatal.4c03065
ACS Catal. 2024, 14, 13640−13651

constraints, and finally 10 ps, with harmonic restraints on QM heavy atoms. The SHAKE algorithm was used for the hydrogen atoms. It was then equilibrated with QM on for 15 ps with harmonic restraints; then we removed the harmonic constraints, and equilibration ran for 60 ps.

For the second step of acylation, we took the final structure of the tetrahedral intermediate from a reactive TPS trajectory and performed equilibration.

Transition Path Sampling. With our equilibrated structures, transition path sampling simulations were used to generate ensembles of reactive trajectories. The QM atoms were specifically labeled, as shown in Figure 13.

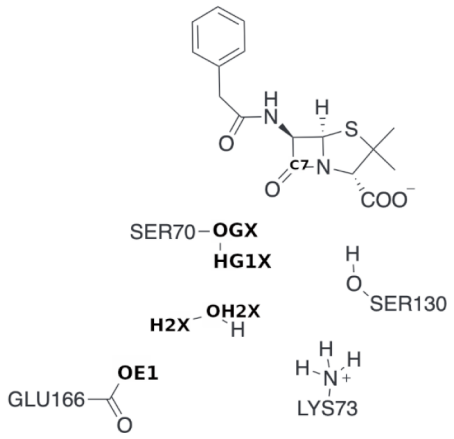

Figure 13. Labeled QM atoms are used to define order parameters for TPS for the formation of the tetrahedral intermediate.

First, we defined order parameters: the preacylation reactant state consists of the Ser70 and benzylpenicillin β-lactam ring carbon distance remaining OGX−C7 > 1.6 Å, the Ser70 oxygen−hydrogen donor bond OGX−HG1X < 1.1 Å, and catalytic water oxygen−hydrogen donor bond OH2X−H2X < 1.1 Å. The product state is defined as OGX−C7 < 1.6 Å, the catalytic water oxygen and Ser70 hydrogen OH2X−HG1X < 1.1 Å, and the Glu166 oxygen and catalytic water hydrogen OE1−H2X < 1.1 Å.

To generate an initial biased trajectory, harmonic constraints were used to force OGX−C7 to a distance of 1.45 Å with a force constant of 16 kcal/mol, OH2X−HG1X to 1.0 Å at 8 kcal/mol, and OE1−H2X at 1.0 Å at 5 kcal/mol. This 500 fs generated trajectory connects the reactant state to the product state. It contains the two proton transfers, and then the Ser70 nucleophile attacks the carbonyl and is then subjected to the shooting algorithm.[50] At a random time slice along this biased trajectory, we perturb the momenta randomly drawing from a Boltzmann distribution, and a new trajectory propagates backward and forward in time for 250 fs. Over 150 reactive trajectories were generated to make up the transition path ensemble.

Committor analysis was used to generate our transition state ensemble.[34] Along the reactive trajectory, we generate momenta randomly from a Boltzmann distribution at each time slice approaching the expected transition state, and the system again propagates forward and backward. We repeated this process 50 times for each random slice and recorded the results of that slice committed to the reactant or the product state. We identified the isocommittor point in each reactive trajectory, the point along the reactive trajectory that has a 0.5 probability of committing to either the reactant state or the product state, which is our transition state. The collection of isocommittor points from the reactive trajectories makes up the separatrix.[51] For the ancestral GNCA enzyme, there was one isocommittor point, or transition state, found, but the modern TEM-1 β-lactamase has two isocommittor points corresponding to sequential transfers.

To find the reaction coordinate residues, we guessed a set of residues to constrain and perform a committor analysis. These residues are a collection of the degrees of freedom required for the reaction to reach the transition state and are orthogonal to the stochastic separatrix.[52] We generated a 250 fs trajectory with the candidate reaction coordinate residues constrained, starting from an identified transition state. We ran dynamics at points along this trajectory, generating random momenta from a Boltzmann distribution and then performed committor analysis on those "constrained-walk" trajectories. If the correct reaction coordinate residues were constrained, then the probability of each point along this constrained-walk trajectory would peak at 0.5.[51] If it does not peak at 0.5, we repeat the process again with a new guess for the reaction coordinate residues. This process was continued until we found two sets of residues for each enzyme that cause the commitment distribution histograms to peak at 0.5. In the case of the modern enzyme, an additional reaction coordinate was found for the second isocommittor point.

The same procedures were performed for acylation of the tetrahedral intermediate step as well. Figure 14 shows the essential labeled atoms for the order parameters for the second step.

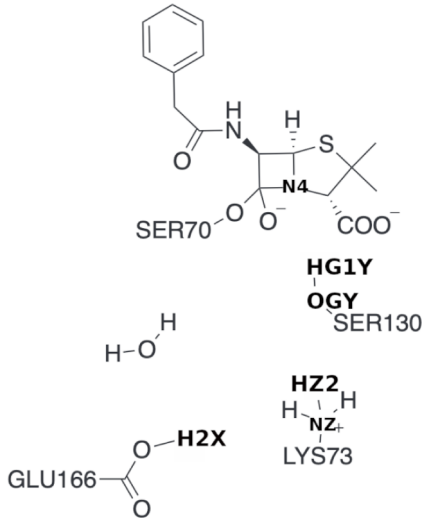

Figure 14. QM region with donor−acceptor atoms labeled for the second step.

The initial biased trajectories were generated by using harmonic constraints to force Lys73 NZ−H2X to a distance of 1.1 Å with a force constant of 15 kcal/mol, HZ2−OGY to 1.1 Å at 11 kcal/mol, and HG1Y−N4 at 1.0 Å at 9 kcal/mol. The reactant state order parameters for the modern TEM-1 distances are as followed: the Glu166 oxygen and catalytic water hydrogen OE1−H2X < 1.25 Å, Lys73 NZ−HZ1 < 1.25 Å, and Ser130 OGY−HG1Y < 1.25 Å. The product state is determined once the three protons are transferred: H2X−NZ

https://doi.org/10.1021/acscatal.4c03065
ACS Catal. 2024, 14, 13640−13651

< 1.25 Å, OGY−HZ1 1.25 Å, and benzylpenicillin N4−HG1Y 1.25 Å.

The ancestral enzyme is slightly different, due to the first donor−acceptor pair of the Glu166 H2X and Lys73 NZ. This transfer occurs instantly, within 5 fs of the trajectory, making it impossible to perform the shooting algorithm on a biased trajectory including this transfer. Therefor we defined the following order parameters for the final acylation step in the ancestral enzyme: Lys73 NZ-HZ2 < 1.25 Å, Ser130 OGY-HG1Y < 1.25 Å. The product state is defined after the transfers, so that HZ2-OGY < 1.25 Å and benzylpenicillin N4-HG1Y < 1.25 Å. Following the initial biased trajectory, the transition path ensembles were formed and then committor analysis was performed to identify the transition states, and finally reaction coordinate residues were found using the same method as in step 1.

Electric Field Calculations. We studied the electrostatic interactions in the active site by calculating the electric field along the substrate's C15═O16 carbonyl. The charges that make up the active site in this case came from the superposition of all electrostatic contributions from the QM region as well as the rest of the classical atom protein within a cutoff of 12 Å. For both systems, ancestral GNCA and TEM-1 β-lactamase, we calculated the Mulliken charges before, during, and after transition state formation for multiple reactive trajectories. The forces projected along the benzylpenicillin carbonyl come from all atoms in the active site along with the classical atoms with a cutoff of 12 Å:

$$\vec{E_j} = \sum_i \text{charge}_i \cdot \frac{\vec{R_i} - \vec{R_j}}{|\vec{R_i} - \vec{R_j}|^3} \quad (1)$$

The contributions of charges i are summed to produce the field on point j. We calculated the field on C15 and a separate field on O16 to find the projection along the C15═O16 axis. The electric field on the dipole is the result of 1/2 the sum of the two fields on C15 and O16. The configuration of the active site is responsible for the electric field.[20,53] The process was repeated in an identical manner for both systems and both steps.

AUTHOR INFORMATION

Corresponding Author

Steven D. Schwartz − *Department of Chemistry & Biochemistry, University of Arizona, Tucson, Arizona 85721, United States;* orcid.org/0000-0002-0308-1059; Email: sschwartz@arizona.edu

Authors

Clara F. Frost − *Department of Chemistry & Biochemistry, University of Arizona, Tucson, Arizona 85721, United States*

Dimitri Antoniou − *Department of Chemistry & Biochemistry, University of Arizona, Tucson, Arizona 85721, United States*

Complete contact information is available at: https://pubs.acs.org/10.1021/acscatal.4c03065

Notes

The authors declare no competing financial interest.

ACKNOWLEDGMENTS

All computer simulations were performed at the University of Arizona High Performance Computing Center, on a Penguin Altus XE2242 supercomputer. This research was supported through the NIH grant R35GM145213.

REFERENCES

(1) Jackson, C. J.; Foo, J.-L.; Tokuriki, N.; Afriat, L.; Carr, P. D.; Kim, H.-K.; Schenk, G.; Tawfik, D. S.; Ollis, D. L. Conformational Sampling, Catalysis, and Evolution of the Bacterial Phosphotriesterase. *Proc. Natl. Acad. Sci. U. S. A.* **2009**, *106* (51), 21631−21636.

(2) Henzler-Wildman, K.; Kern, D. Dynamic Personalities of Proteins. *Nature* **2007**, *450* (7172), 964−972.

(3) Schafer, J. W.; Zoi, I.; Antoniou, D.; Schwartz, S. D. Optimization of the Turnover in Artificial Enzymes via Directed Evolution Results in the Coupling of Protein Dynamics to Chemistry. *J. Am. Chem. Soc.* **2019**, *141* (26), 10431−10439.

(4) Gumulya, Y.; Gillam, E. M. J. Exploring the Past and the Future of Protein Evolution with Ancestral Sequence Reconstruction: The 'Retro' Approach to Protein Engineering. *Biochem. J.* **2017**, *474* (1), 1−19.

(5) Perez-Garcia, P.; Kobus, S.; Gertzen, C. G. W.; Hoeppner, A.; Holzscheck, N.; Strunk, C. H.; Huber, H.; Jaeger, K.-E.; Gohlke, H.; Kovacic, F.; et al. A promiscuous ancestral enzymés structure unveils protein variable regions of the highly diverse metallo-β-lactamase family. *Commun. Biol.* **2021**, *4* (1), 132.

(6) Petrović, D.; Risso, V. A.; Kamerlin, S. C. L.; Sanchez-Ruiz, J. M. Conformational Dynamics and Enzyme Evolution. *J. R. Soc., Interface* **2018**, *15* (144), 20180330.

(7) Modi, T.; Campitelli, P.; Heyden, M.; Ozkan, S. B. Correlated Evolution of Low-Frequency Vibrations and Function in Enzymes. *J. Phys. Chem. B* **2023**, *127* (3), 616−622.

(8) Risso, V. A.; Martinez-Rodriguez, S.; Candel, A. M.; Krüger, D. M.; Pantoja-Uceda, D.; Ortega-Muñoz, M.; Santoyo-Gonzalez, F.; Gaucher, E. A.; Kamerlin, S. C. L.; Bruix, M.; et al. De Novo Active Sites for Resurrected Precambrian Enzymes. *Nat. Commun.* **2017**, *8* (1), 16113.

(9) Risso, V. A.; Gavira, J. A.; Mejia-Carmona, D. F.; Gaucher, E. A.; Sanchez-Ruiz, J. M. Hyperstability and Substrate Promiscuity in Laboratory Resurrections of Precambrian β-Lactamases. *J. Am. Chem. Soc.* **2013**, *135* (8), 2899−2902.

(10) Modi, T.; Risso, V. A.; Martinez-Rodriguez, S.; Gavira, J. A.; Mebrat, M. D.; Van Horn, W. D.; Sanchez-Ruiz, J. M.; Banu Ozkan, S. Hinge-Shift Mechanism as a Protein Design Principle for the Evolution of β-Lactamases from Substrate Promiscuity to Specificity. *Nat. Commun.* **2021**, *12* (1), 1852.

(11) Zou, T.; Risso, V. A.; Gavira, J. A.; Sanchez-Ruiz, J. M.; Ozkan, S. B. Evolution of Conformational Dynamics Determines the Conversion of a Promiscuous Generalist into a Specialist Enzyme. *Mol. Biol. Evol.* **2015**, *32* (1), 132−143.

(12) Hermann, J. C.; Hensen, C.; Ridder, L.; Mulholland, A. J.; Höltje, H.-D. Mechanisms of Antibiotic Resistance: QM/MM Modeling of the Acylation Reaction of a Class A β-Lactamase with Benzylpenicillin. *J. Am. Chem. Soc.* **2005**, *127* (12), 4454−4465.

(13) Ji, Z.; Boxer, S. G. β-Lactamases Evolve against Antibiotics by Acquiring Large Active-Site Electric Fields. *J. Am. Chem. Soc.* **2022**, *144* (48), 22289−22294.

(14) Minasov, G.; Wang, X.; Shoichet, B. K. An Ultrahigh Resolution Structure of TEM-1 β-Lactamase Suggests a Role for Glu166 as the General Base in Acylation. *J. Am. Chem. Soc.* **2002**, *124* (19), 5333−5340.

(15) Hermann, J. C.; Ridder, L.; Höltje, H.-D.; Mulholland, A. J. Molecular Mechanisms of Antibiotic Resistance: QM/MM Modelling of Deacylation in a Class A β-Lactamase. *Org. Biomol. Chem.* **2006**, *4* (2), 206−210.

(16) Langan, P. S.; Vandavasi, V. G.; Cooper, C. J.; Weiss, K. L.; Ginell, S. L.; Parks, J. M.; Coates, L. Substrate Binding Induces Conformational Changes in a Class A β-Lactamase That Prime It for Catalysis. *ACS Catal.* **2018**, *8* (3), 2428−2437.

(17) Meroueh, S. O.; Fisher, J. F.; Schlegel, H. B.; Mobashery, S. Ab Initio QM/MM Study of Class A β-Lactamase Acylation: Dual

Participation of Glu166 and Lys73 in a Concerted Base Promotion of Ser70. *J. Am. Chem. Soc.* **2005**, *127* (44), 15397−15407.
(18) Banerjee, S.; Pieper, U.; Kapadia, G.; Pannell, L. K.; Herzberg, O. Role of the Ω-Loop in the Activity, Substrate Specificity, and Structure of Class A β-Lactamase. *Biochemistry* **1998**, *37* (10), 3286−3296.
(19) Egorov, A.; Rubtsova, M.; Grigorenko, V.; Uporov, I.; Veselovsky, A. The Role of the Ω-Loop in Regulation of the Catalytic Activity of TEM-Type β-Lactamases. *Biomolecules* **2019**, *9* (12), 854.
(20) Fried, S. D.; Boxer, S. G. Electric Fields and Enzyme Catalysis. *Annu. Rev. Biochem.* **2017**, *86* (1), 387−415.
(21) Fried, S. D.; Bagchi, S.; Boxer, S. G. Extreme Electric Fields Power Catalysis in the Active Site of Ketosteroid Isomerase. *Science* **2014**, *346* (6216), 1510−1514.
(22) Suydam, I. T.; Snow, C. D.; Pande, V. S.; Boxer, S. G. Electric Fields at the Active Site of an Enzyme: Direct Comparison of Experiment with Theory. *Science* **2006**, *313* (5784), 200−204.
(23) Núñez, S.; Wing, C.; Antoniou, D.; Schramm, V. L.; Schwartz, S. D. Insight into Catalytically Relevant Correlated Motions in Human Purine Nucleoside Phosphorylase. *J. Phys. Chem. A* **2006**, *110* (2), 463−472.
(24) Masterson, J. E.; Schwartz, S. D. Changes in Protein Architecture and Subpicosecond Protein Dynamics Impact the Reaction Catalyzed by Lactate Dehydrogenase. *J. Phys. Chem. A* **2013**, *117* (32), 7107−7113.
(25) Kalyanaraman, C.; Schwartz, S. D. Effect of Active Site Mutation Phe 93 → Trp in the Horse Liver Alcohol Dehydrogenase Enzyme on Catalysis: A Molecular Dynamics Study. *J. Phys. Chem. B* **2002**, *106* (51), 13111−13113.
(26) Saen-Oon, S.; Ghanem, M.; Schramm, V. L.; Schwartz, S. D. Remote Mutations and Active Site Dynamics Correlate with Catalytic Properties of Purine Nucleoside Phosphorylase. *Biophys. J.* **2008**, *94* (10), 4078−4088.
(27) Harijan, R. K.; Zoi, I.; Antoniou, D.; Schwartz, S. D.; Schramm, V. L. Inverse Enzyme Isotope Effects in Human Purine Nucleoside Phosphorylase with Heavy Asparagine Labels. *Proc. Natl. Acad. Sci. U. S. A.* **2018**, *115* (27), No. E6209-E6216.
(28) Schafer, J. W.; Schwartz, S. D. Directed Evolution's Influence on Rapid Density Fluctuations Illustrates How Protein Dynamics Can Become Coupled to Chemistry. *ACS Catal.* **2020**, *10* (15), 8476−8484.
(29) Chen, X.; Schwartz, S. D. Directed Evolution as a Probe of Rate Promoting Vibrations Introduced via Mutational Change. *Biochemistry* **2018**, *57* (23), 3289−3298.
(30) Balasubramani, S. G.; Korchagina, K.; Schwartz, S. Transition Path Sampling Study of Engineered Enzymes That Catalyze the Morita−Baylis−Hillman Reaction: Why Is Enzyme Design so Difficult? *J. Chem. Inf. Model.* **2024**, *64* (6), 2101−2111.
(31) Frost, C. F.; Balasubramani, S. G.; Antoniou, D.; Schwartz, S. D. Connecting Conformational Motions to Rapid Dynamics in Human Purine Nucleoside Phosphorylase. *J. Phys. Chem. B* **2023**, *127* (1), 144−150.
(32) Bunzel, H. A.; Anderson, J. L. R.; Hilvert, D.; Arcus, V. L.; Van Der Kamp, M. W.; Mulholland, A. J. Evolution of Dynamical Networks Enhances Catalysis in a Designer Enzyme. *Nat. Chem.* **2021**, *13* (10), 1017−1022.
(33) Dellago, C.; Bolhuis, P. G.; Csajka, F. S.; Chandler, D. Transition Path Sampling and the Calculation of Rate Constants. *J. Chem. Phys.* **1998**, *108* (5), 1964−1977.
(34) Schwartz, S. D. Protein Dynamics and the Enzymatic Reaction Coordinate. In *Dynamics in Enzyme Catalysis*; Klinman, J.; Hammes-Schiffer, S.;Springer: Berlin, Heidelberg, 2013; Vol. *337*, pp. 189208.
(35) Schneider, S. H.; Kozuch, J.; Boxer, S. G. The Interplay of Electrostatics and Chemical Positioning in the Evolution of Antibiotic Resistance in TEM β-Lactamases. *ACS Cent. Sci.* **2021**, *7* (12), 1996−2008.
(36) Fisette, O.; Gagné, S.; Lagüe, P. Molecular Dynamics of Class A β-Lactamases-Effects of Substrate Binding. *Biophys. J.* **2012**, *103* (8), 1790−1801.
(37) Zoi, I.; Antoniou, D.; Schwartz, S. D. Electric Fields and Fast Protein Dynamics in Enzymes. *J. Phys. Chem. Lett.* **2017**, *8* (24), 6165−6170.
(38) Ponder, J. W.; Wu, C.; Ren, P.; Pande, V. S.; Chodera, J. D.; Schnieders, M. J.; Haque, I.; Mobley, D. L.; Lambrecht, D. S.; DiStasio, R. A.; Head-Gordon, M.; Clark, G. N. I.; Johnson, M. E.; Head-Gordon, T. Current Status of the AMOEBA Polarizable Force Field. *J. Phys. Chem. B* **2010**, *114* (8), 2549−2564.
(39) Guan, X.; Leven, I.; Heidar-Zadeh, F.; Head-Gordon, T. Protein C-GeM: A Coarse-Grained Electron Model for Fast and Accurate Protein Electrostatics Prediction. *J. Chem. Inf. Model.* **2021**, *61* (9), 4357−4369.
(40) Hermann, J. C.; Ridder, L.; Mulholland, A. J.; Höltje, H.-D. Identification of Glu166 as the General Base in the Acylation Reaction of Class A β-Lactamases through QM/MM Modeling. *J. Am. Chem. Soc.* **2003**, *125* (32), 9590−9591.
(41) Brown, N. G.; Shanker, S.; Prasad, B. V. V.; Palzkill, T. Structural and Biochemical Evidence That a TEM-1 β-Lactamase N170G Active Site Mutant Acts via Substrate-Assisted Catalysis. *J. Biol. Chem.* **2009**, *284* (48), 33703−33712.
(42) Balasubramani, S. G.; Schwartz, S. D. Transition Path Sampling Based Calculations of Free Energies for Enzymatic Reactions: The Case of Human Methionine Adenosyl Transferase and *Plasmodium Vivax* Adenosine Deaminase. *J. Phys. Chem. B* **2022**, *126* (29), 5413−5420.
(43) Schrödinger *Release 2023−3: Maestro*; Schrödinger, LLC, New York, NY, 2023.
(44) Brooks, B. R.; Bruccoleri, R. E.; Olafson, B. D.; States, D. J.; Swaminathan, S.; Karplus, M. CHARMM: A Program for Macromolecular Energy, Minimization, and Dynamics Calculations. *J. Comput. Chem.* **1983**, *4* (2), 187−217.
(45) Brooks, B. R.; Brooks, C. L.; Mackerell, A. D.; Nilsson, L.; Petrella, R. J.; Roux, B.; Won, Y.; Archontis, G.; Bartels, C.; Boresch, S.; Caflisch, A.; Caves, L.; Cui, Q.; Dinner, A. R.; Feig, M.; Fischer, S.; Gao, J.; Hodoscek, M.; Im, W.; Kuczera, K.; Lazaridis, T.; Ma, J.; Ovchinnikov, V.; Paci, E.; Pastor, R. W.; Post, C. B.; Pu, J. Z.; Schaefer, M.; Tidor, B.; Venable, R. M.; Woodcock, H. L.; Wu, X.; Yang, W.; York, D. M.; Karplus, M. CHARMM: The Biomolecular Simulation Program. *J. Comput. Chem.* **2009**, *30* (10), 1545−1614.
(46) Jorgensen, W. L.; Chandrasekhar, J.; Madura, J. D.; Impey, R. W.; Klein, M. L. Comparison of Simple Potential Functions for Simulating Liquid Water. *J. Chem. Phys.* **1983**, *79* (2), 926−935.
(47) Vanommeslaeghe, K.; Hatcher, E.; Acharya, C.; Kundu, S.; Zhong, S.; Shim, J.; Darian, E.; Guvench, O.; Lopes, P.; Vorobyov, I.; Mackerell, A. D. CHARMM General Force Field: A Force Field for Drug-like Molecules Compatible with the CHARMM All-atom Additive Biological Force Fields. *J. Comput. Chem.* **2010**, *31* (4), 671−690.
(48) Gao, J.; Amara, P.; Alhambra, C.; Field, M. J. A Generalized Hybrid Orbital (GHO) Method for the Treatment of Boundary Atoms in Combined QM/MM Calculations. *J. Phys. Chem. A* **1998**, *102* (24), 4714−4721.
(49) BIOVIA Discovery Studio *Discovery Studio Visualizer*; BIOVIA Discovery Studio: San Diego, 2019.
(50) Bolhuis, P. G.; Chandler, D.; Dellago, C.; Geissler, P. L. TRANSITION PATH SAMPLING: Throwing Ropes Over Rough Mountain Passes, in the Dark. *Annu. Rev. Phys. Chem.* **2002**, *53* (1), 291−318.
(51) Antoniou, D.; Schwartz, S. D. The Stochastic Separatrix and the Reaction Coordinate for Complex Systems. *J. Chem. Phys.* **2009**, *130* (15), 151103.
(52) Antoniou, D.; Abolfath, M. R.; Schwartz, S. D. Transition Path Sampling Study of Classical Rate-Promoting Vibrations. *J. Chem. Phys.* **2004**, *121* (13), 6442−6447.
(53) Warshel, A.; Sharma, P. K.; Kato, M.; Xiang, Y.; Liu, H.; Olsson, M. H. M. Electrostatic Basis for Enzyme Catalysis. *Chem. Rev.* **2006**, *106* (8), 3210−3235.

https://doi.org/10.1021/acscatal.4c03065
ACS Catal. 2024, 14, 13640−13651